Electric Power Systems Research 81 (2011) 308–317

Contents lists available at ScienceDirect

Electric Power Systems Research

journal homepage: www.elsevier.com/locate/epsr

Damping of sub-synchronous resonance and low-frequency power oscillation in a series-compensated transmission line using gate-controlled series capacitor

Mohammad Reza Alizadeh Pahlavani*, Hossein Ali Mohammadpour

Department of Electrical Engineering, Iran University of Science and Technology (IUST), Heidarkhani St., Narmak, 16844 Tehran, Iran

ARTICLE INFO

Article history:
Received 4 March 2010
Received in revised form 26 June 2010
Accepted 21 September 2010
Available online 3 November 2010

Keywords:
Flexible AC transmission systems (FACTS)
Fuzzy logic
Gate-controlled series capacitor
Low-frequency power oscillation
Sub-synchronous resonance (SSR)

ABSTRACT

In this paper, the impact of different gate-controlled series capacitor (GCSC) control methodologies on sub-synchronous resonance (SSR) problems of series capacitive compensated transmission lines is analyzed. The low-frequency power oscillation (LFPO) damping using GCSC also is studied. In these studies, the effect of the rating of the GCSC is also considered. Three different control methodologies are proposed: open loop, constant power, and Takagi-Sugeno (TS) fuzzy control. It is shown that the GCSC can damp both the SSR and LFPO using the constant power control (CPC) methodology. It is also shown that when the parameters of the CPC is optimized by the TS fuzzy controller, the third methodology can present a cost-effective solution for both the SSR and LFPO damping. In this work, the IEEE First Benchmark Model is employed, including a GCSC device, and the study is performed using MATLAB program.

1. Introduction

SERIES capacitors have extensively been used as a very effective means of increasing the power transfer capability of a transmission lines and improving transient and steady state stability limits of power systems. This is due to partially compensating the reactance of the transmission lines. However, capacitors in series with transmission lines may cause sub-synchronous resonance (SSR) problems. SSR problems result from the interaction between an electrical mode of the series compensated network and a mechanical shaft mode of a turbine-generator group, which can lead to turbine-generator shaft failure and electrical instability at oscillation frequencies lower than the normal system frequency [1,2].

Flexible AC transmission systems (FACTS) controllers such as the static synchronous compensator (STATCOM) [3], the static synchronous series compensator (SSSC) [4,5], the unified power flow controller (UPFC) [6], and the thyristor controlled series capacitor (TCSC) [7] have been applied to prevent the SSR in power systems.

The gate-controlled series capacitor (GCSC) is a series FACTS device proposed initially for series compensation in transmission lines to control power flow [8,9]. It was shown that with the proper turn-off angle control of the GCSC, this device can damp SSR [10]. Moreover, in [11,12], a further investigation of the capability of the GCSC with respect to SSR as well as LFPO damping was presented, and in these investigations, the effect of the rating of the GCSC also was considered, and the GCSC with the small, the medium, and the large ratings were studied.

This paper presents a detailed analysis of the impact of different GCSC control methodologies on SSR and LFPO damping. For this analysis, three different control methodologies are proposed:

(1) Open loop control;
(2) Constant power control (CPC);
(3) Takagi-Sugeno (TS) fuzzy logic control.

In addition, the analysis studies the effect of the rating of the GCSC so that two different GCSC ratings are considered. The considered GCSC ratings are the small and large ratings considered in [11,12].

The structure of the paper is as follows: in Section 2 the studied power system is introduced; in Section 3 the stability of the power system is analyzed; in Section 4 the results of the fixed series compensation is given; in Section 5 the principle operation of the GCSC is briefly presented, and this device is compared with the TCSC; in Sections 6 and 7 the GCSC open loop control and CPC methodologies are proposed, respectively, and in section 8 the results of the application of TS fuzzy controller in the GCSC is shown, and to validate the obtained results, these results are compared with the best results of Refs. [11,12].

* Corresponding author. Tel.: +98 2123812522/9123192585; fax: +98 2177240490.
E-mail address: Mr_Alizadehp@iust.ac.ir (M.R. Alizadeh Pahlavani).

0378-7796/$ – see front matter.
doi:10.1016/j.epsr.2010.09.007

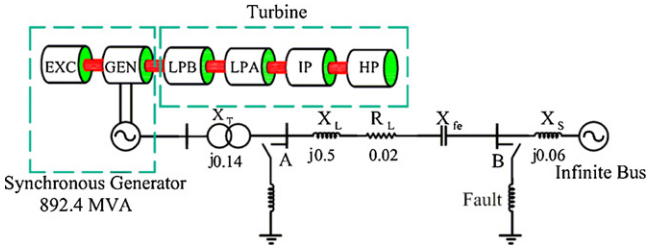

Fig. 1. IEEE First Benchmark Model.

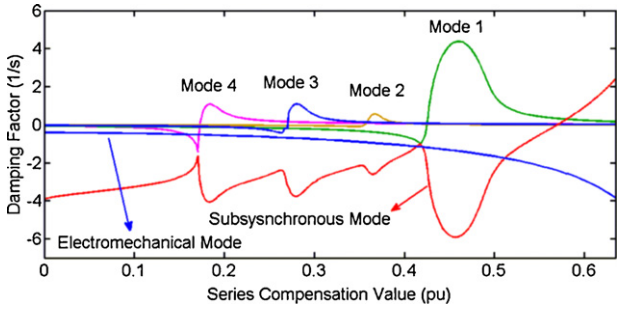

Fig. 2. Damping factors of the studied system as a function of the series compensation value.

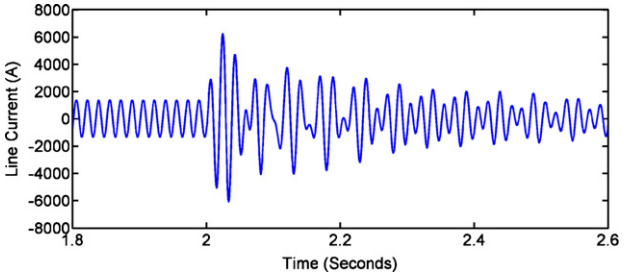

Fig. 3. Line current response with fixed series compensation.

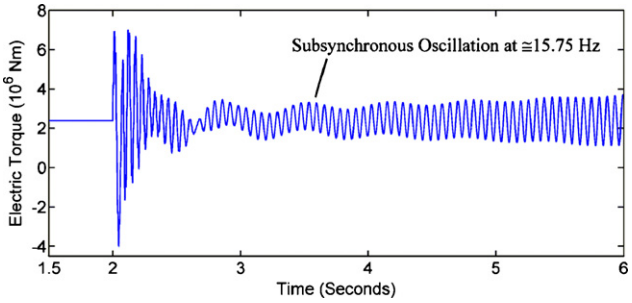

Fig. 4. Electric torque response with fixed series.

2. Power system study model

For the analysis presented in this paper, the IEEE First Benchmark Model (FBM) is employed, which is shown in Fig. 1. In this model, an 892.4 MVA synchronous generator is connected to an infinite bus via a 500 kV compensated transmission line. The transmission line is represented by a resistance, a reactance, and a series fixed capacitive compensation, X_{fc}. The complete electrical and mechanical data for this model are presented in [2].

3. Eigenvalue analysis

For an assessment of the dynamic characteristics of the system, the eigenvalues are obtained by M-file in the MATLAB program. In Fig. 2 the damping factor of the SSR modes of the system as a function of the series compensation value is shown. As seen in this figure, the system has four unstable torsional modes. Also, in Table 1 the frequency and the corresponding damping factor as well as the value of series compensation associated with the maximum torsional interactions are given. Fig. 2 shows that the worst situation for SSR damping is when the system is tuned at torsional mode 1; hence, in this paper, the effect of the presented control methodologies will be investigated when the system is tuned at this mode.

4. Fixed series compensation

The system was tuned to the torsional mode 1 based on Table 1. Then the simulation of the system in Fig. 1 was started with an ideal voltage source on the generator side, and at $t = 2$ s the ideal voltage source was substituted by the synchronous generator driven by the six-stage turbine generator as shown in Fig. 1 while at the same time a three-phase fault was applied at point B (see Fig. 1). Figs. 3 and 4 show the unstable line current and the electric torque of the system, respectively. The electric torque response shows that the main oscillation occurs at around 15.75 Hz, which is the frequency of oscillation of torsional mode 1, as given in Table 1.

Table 1
Frequency of oscillation and capacitive reactance of the maximum torsional interactions.

Mode	Frequency (Hz)	Damping factor (1/s)	X_{fc} (p.u.)
Torsional 1	15.75	4.323	0.472
Torsional 2	20.41	0.404	0.378
Torsional 3	25.55	1.051	0.285
Torsional 4	32.29	1.066	0.164
Low-frequency	0.5–2.5	–	–

5. The GCSC and its Comparison with the TCSC

The first generation of FACTS devices for series compensation consisted of a variable impedance-type compensator based on thyristors. This device, known as a thyristor-controlled series capacitor (TCSC), uses a thyristor-controlled reactor (TCR) in parallel with a fixed capacitor, as shown in Fig. 5. The thyristor-controlled series capacitor (TCSC) is a commercially available flexible ac transmission system (FACTS) device developed for controlled compensation of transmission-line impedance, which consequently leads to the control of transmission- line power flow. Fig. 6 shows a typical impedance curve for a TCSC, as a function of the firing angle α. $X_{MAX-TCSC}$ is the maximum values of the impedance of the TCSC operating in the capacitive region. This value

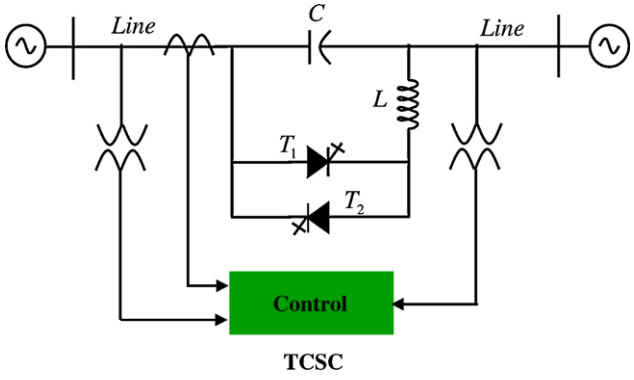

Fig. 5. Basic configuration of the TCSC.

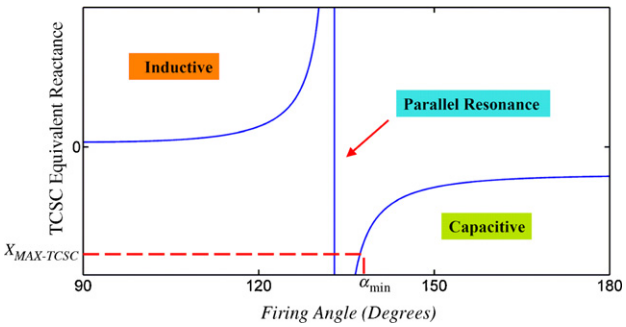

Fig. 6. Equivalent reactance of the TCSC as a function of firing angle.

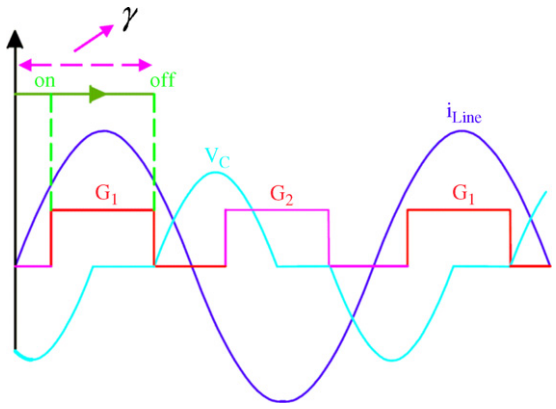

Fig. 7. GCSC voltage, current, and switch control.

corresponds to the equivalent impedance of the TCSC for the minimum firing angle α_{min}. This angle is limited in order to avoid the potentially dangerous operation near the parallel resonance region. The internal parallel resonance is also shown in this figure. By varying the firing angle of the thyristor, the parallel LC circuit is tuned, resulting in controllable equivalent impedance. Care must be taken when tuning the firing angle, to avoid parallel resonance of the controllable reactor and the capacitor.

A second generation of series compensation devices uses gate turnoff (GTO) or other symmetrical gate-commutated switches to continuously regulate the capacitor voltage. Fig. 7 shows the current and voltage waveforms of the GCSC. Also in Fig. 8 the basic configuration of the GCSC is shown. The principle of GCSC operation is based on the variation of the turn-off angle (γ) of the gate-controlled switches [12–16]. By controlling the turn-off angle (γ), the voltage on the capacitor is controlled; as a result, the series compensation level of the transmission line can be controlled. The

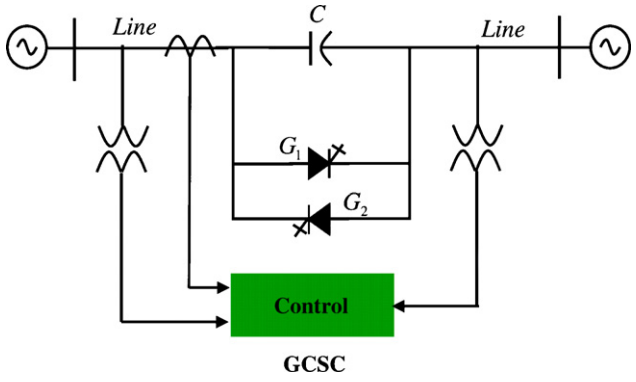

Fig. 8. Basic configuration of the GCSC.

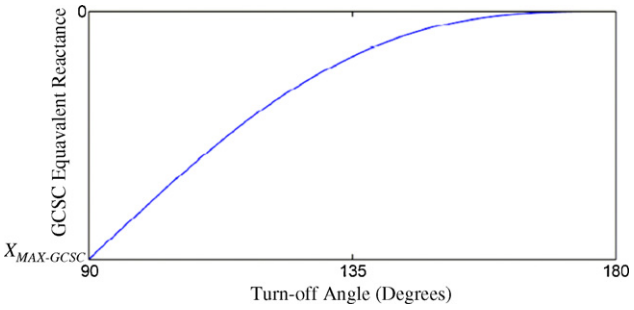

Fig. 9. Equivalent reactance of the GCSC as a function of turn-off angle.

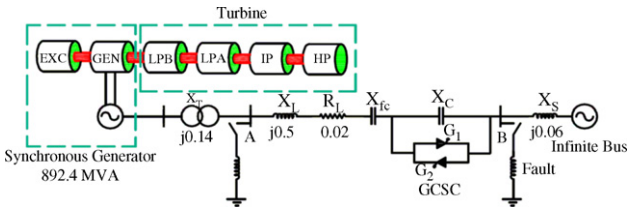

Fig. 10. IEEE First Benchmark Model with GCSC.

turn-off angle (γ) is measured from the zero crossing of the line current, and the compensation level of the GCSC is determined by the fundamental component of the voltage (v_C) on the GCSC. The relationship between equivalent capacitive reactance and turn-off angle (γ) is given by [12–16]:

$$X(\gamma) = \frac{X_C}{\pi}(2\gamma - 2\pi - \sin(2\gamma)) \quad (1)$$

where X_C is the reactance of the GCSC capacitor.

Fig. 9 shows typical impedance characteristic of the GCSC, as a function of the turn-off angle. In this figure, $X_{MAX-GCSC}$ represents the maximum values of the impedance of the GCSC and is obtained with a turn-off angle equals to 90°.

In many situations where a controllable series compensator must be installed, the GCSC may be used instead of the TCSC, possibly with some advantages. A comparison of the sizing of the TCSC and the GCSC components, when both the GCSC and the TCSC have the same maximum capacitive impedance ($X_{MAX-TCSC} = X_{MAX-GCSC}$), shows that the capacitor in the GCSC can have lower megavolt-amperes than in the TCSC, especially for power-flow control applications. Also, the thyristor valve in the TCSC needs to have a higher current rating than the gate-commutated switch valve in the GCSC. Moreover, the components of a GCSC designed for the same maximum compensation level of a TCSC may have switches with a smaller rating and, naturally, will not need the reactor; hence, unlike the TCSC, the GCSC does not have any intrinsic internal resonance [9].

5.1. Series compensation with the GCSC

A GCSC device was substituted for a portion of the fixed series compensation in the IEEE FBM, as seen in Fig. 10. The total capacitive series compensation was made equal to 0.472 p.u. just to try to excite the SSR at mode 1, as given in Table 1. In [11,12], the proportion between the GCSC equivalent reactance and the fixed capacitor reactance was considered in three cases, which are given in Table 2. As seen in this table, for example in Case I (the small rating), the GCSC was designed to provide 0.152 p.u. of the capacitive equivalent reactance and the fixed capacitor provided 0.318 p.u. Then it was shown that the higher rating of the GCSC (Cases II and III), the better and the easier SSR damping. Among the aforementioned three cases, Case I is the lowest-cost configuration for the GCSC

Table 2
Compensation cases with the GCSC.

Case	X_{fc} (p.u.)	$X(\gamma)$ (p.u.)
(The small rating) I	0.318	0.152
(The medium rating) II	0.236	0.236
(The large rating) III	0.152	0.318

because the power rating of the GCSC in this case is reduced, while in Case III, the power rating of the GCSC is increased, making this case the highest-cost configuration.

In this paper, Cases I and III, which are, respectively, the lowest-cost and the highest-cost configurations, are considered. The considered cases are highlighted in Table 2. To determine the steady state GCSC equivalent reactance based on the considered cases; depending on the size of the GCSC capacitive reactance (X_C) and its turn-off angle (γ) as can be verified in (1), there are many different states. In this study, the steady state turn-off angle is set at 113.5°, and then the GCSC equivalent reactance can be verified in (1) by setting X_C.

Three control methodologies for turn-off angle control of the GCSC using the cited cases are presented:

- Open loop control;
- Constant power control (CPC);
- Takagi-Sugeno (TS) fuzzy logic control.

The impact of the GCSC on SSR and LFPO damping using these control methodologies is investigated using two kinds of faults as follows:

- A resistive fault by connecting a resistor at point B in Fig. 10 with 0.1 s time duration. This fault is similar to that of the fault applied in [11,12];
- An inductive fault by connecting a reactor at point B in Fig. 10 with 75 ms time duration. This fault, which is stronger than the resistive fault, is the one that have been determined in the IEEE FBM for evaluating the SSR studies.

6. GCSC open loop control

Following the SSR in power systems, the line current frequency will oscillate. The proposed open loop control methodology detects these oscillations and changes the turn-off angle of the GCSC in a way that makes the GCSC able to damp the SSR. Fig. 11 shows the schematic diagram of the GCSC turn-off angle control based on this method. As seen in this figure, this methodology includes four main blocks: a frequency detection block, a turn-off angle estimator block, a pulse generator block, and a decision block. This methodology is described for phase "a" and for other phases, the manner is the same.

As seen in Fig. 11, the frequency detection block is composed of a "Sign" block, a "Zero Comparator," an "Edge" detector, an "Integrator," and an "S/H" block for sampling and holding the data in the specific times. In this block, the phase "a" current is fed to the "Sign" block, producing a square wave signal B, as shown in Fig. 11. Then this square wave is compared with zero to produce signals C and C'. These signals are used to generate pulses for G_1 and G_2, respectively. Here, the pulse generation for G_1 is described. The "Edge" detector generates the reset pulse from signal C for the integrator that is integrating signal C. Using the S/H, the maximum value of the integrator output is obtained giving the half period of line current T_i in positive times of line current. The inverse of this time gives the half frequency of the phase "a" line current in positive times (f_i).

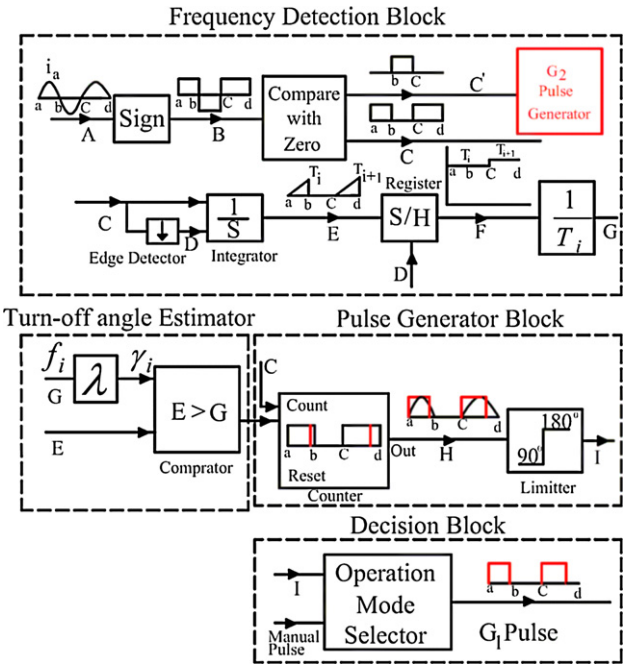

Fig. 11. GCSC open loop control methodology.

Then, in the turn-off angle estimator block, in order to produce the turn-off angle time from f_i, the turn-off angle is obtained using:

$$\gamma_i = \lambda \times f_i \tag{2}$$

The constant parameter λ for the steady state turn-off angle (113.5°) is obtained using:

$$\lambda = \frac{\gamma^*}{f^*} \Rightarrow \lambda = \frac{113.5}{120 \times 180} \times \frac{1}{120} \tag{3}$$

where γ^* is the steady state turn-off angle time and f^* is the half frequency of the steady state line current.

Then, in order to generate the final pulse for G_1, the produced turn-off angle time is compared with the output of the "Integrator" (E), and when the value of E is bigger than the turn-off angle time, a signal is produced to reset the counter, which had been activated by signal C. The output of the counter is passed through a limiter that limits the turn-off angle between 90° and 180°. Finally, in the decision block, there is an operation mode selector that prepares to set a manual constant turn-off angle. This block also decides that either the output of the limiter or the constant turn-off angle is applied to switch G_1 as the turn-off angle time.

6.1. Simulation results and discussions

The simulation of the system shown in Fig. 10 with the proposed control methodology was started with an ideal voltage source on the generator side, and at t = 2 ms, the ideal voltage source was substituted by a synchronous generator driven by the turbine as shown in Fig. 10. Fig. 12 shows the unstable electric torque for Case I, showing that the SSR is present in the system and is visible for times greater than 3 s. This figure shows that with this proportion of the GCSC equivalent reactance $X(\gamma)$ and the fixed capacitor reactance (X_{fc}), the open loop control cannot damp the SSR.

In Fig. 13 the line current response for Case III when the inductive faults is applied at point B in Fig. 10 at t = 7.5 s is shown. As seen in this figure, the inductive fault increases the line current from 1 to about 3.1 p.u. Also, in Figs. 14 and 15, the electrical torque responses of the system for both the resistive and inductive faults are shown. As seen in these figures, the GCSC is able to damp the

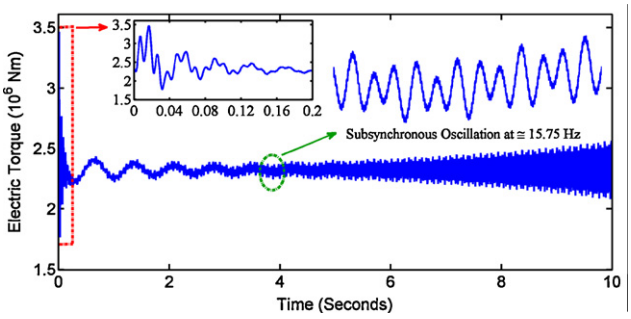

Fig. 12. Electric torque with open loop control (Case I).

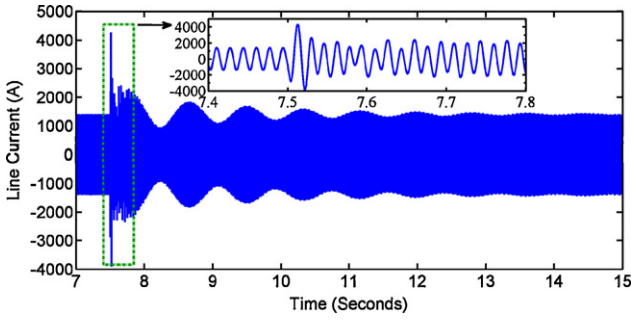

Fig. 13. Line current with open loop control for the inductive fault (Case III).

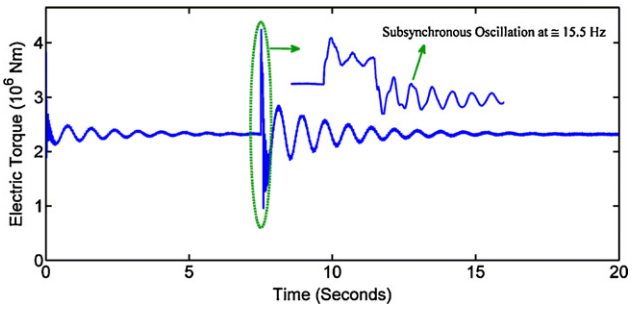

Fig. 14. Electric torque (open loop control for the resistive fault) (Case III).

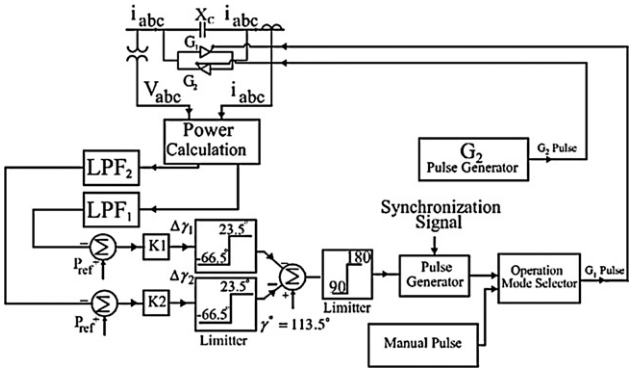

Fig. 16. GCSC with CPC methodology.

SSR and stabilizes the system in Case III using the open loop control methodology.

Based on what already has been discussed, it is concluded that this method is unable to damp the SSR in Case I. It would be better if Case I could stabilize the system, resulting in a lower-cost configuration for the GCSC. However, this method is able to damp the SSR in Case III. Although this shows the ability of the GCSC in SSR damping even with an open loop control methodology, the time duration of the LFPO using this methodology is too long, and for the inductive fault, for example, it lasts for about 7 s, as seen in Fig. 15.

7. GCSC constant power control

Fig. 16 shows the block diagram of the proposed CPC methodology. In this methodology, the power calculation block diagram calculates the line's real power. This measured power is then passed through two first order low-pass filters (LPF_1 and LPF_2). The LPF_1 with cutoff frequency of 3 Hz is used to diagnose the low-frequency power oscillation in the line's real power. Also, the LPF_2 detects the electrical power oscillations with frequencies below 20 Hz, which torsional mode 1 (15.75 Hz) is in this interval.

The outputs of these filters are compared with a power order, and the control errors excite the proportional gains: K_1 and K_2. The output signals of these proportional gains ($\Delta\gamma_1$ and $\Delta\gamma_2$) signify the existence of the SSR and the LFPO in the line's real power, respectively. The sum of $\Delta\gamma_1$ and $\Delta\gamma_2$ with a fixed turn-off angle gives the resulting turn-off angle (γ) of the GCSC. This turn-off angle is passed through a limiter and then is fed to a pulse generator block synchronized by the line's current zero crossing to produce the GCSC's input final pulse. Through the operations described above,

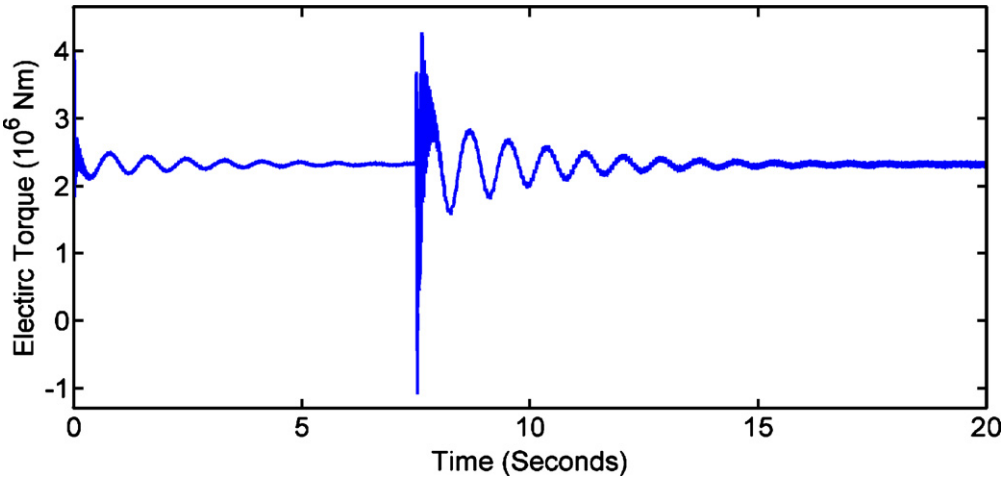

Fig. 15. Electric torque (open loop control for the inductive fault) (Case III).

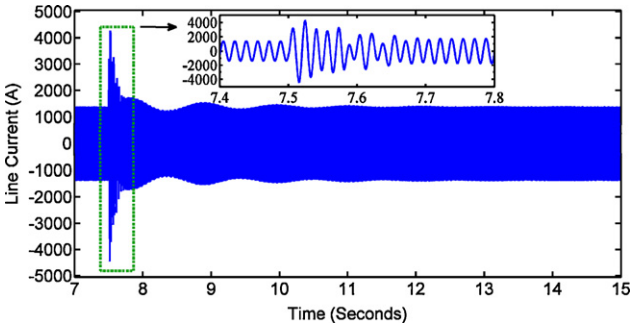

Fig. 17. Line current with CPC for the inductive fault (Case III).

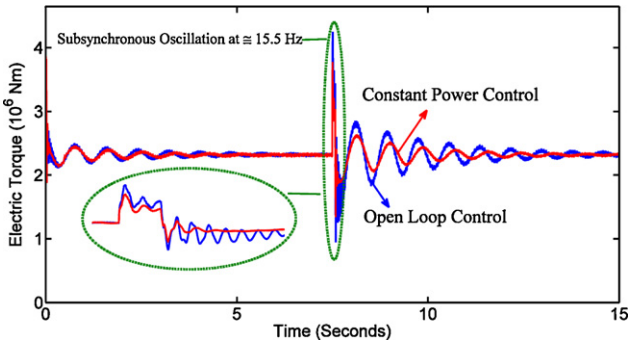

Fig. 18. Electric torque for the resistive fault: GCSC with open loop control and CPC (Case III).

the G_1 pulse is produced. The G_2–G_6 pulses are produced in the same way.

7.1. Simulation results and discussions

The simulation of the system shown in Fig. 10 with the presented closed loop method was started with an ideal voltage source on the generator side, and at $t = 2$ ms, the ideal voltage source was substituted with a synchronous generator driven by the turbine. To investigate the effectiveness of the proposed control methodology, both the resistive and inductive faults were applied at bus B in Fig. 10 at $t = 7.5$ s, and the performance of the GCSC with this control methodology was tested by different gains (K_1, K_2).

For Case III, the best responses for the system were obtained by the gains (0.1, 0.1) [°/MW], and for these gains the resistive fault increased the line current from 1 to about 1.69 p.u., and the inductive fault increased the line current from 1 to about 3.1 p.u. Fig. 17 shows the line current for the inductive fault. Also, in Figs. 18 and 19, the electric torque response corresponding to the resistive and the

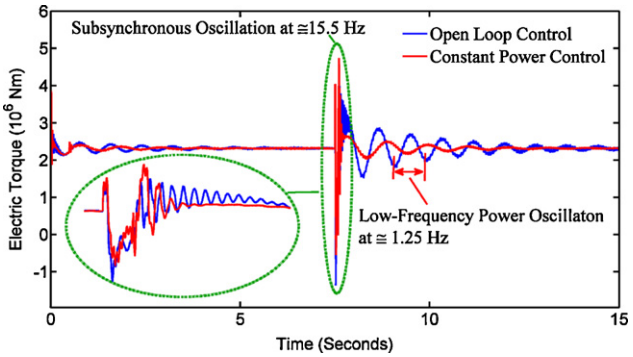

Fig. 19. Electric torque for the inductive fault: GCSC with open loop control and CPC (Case III).

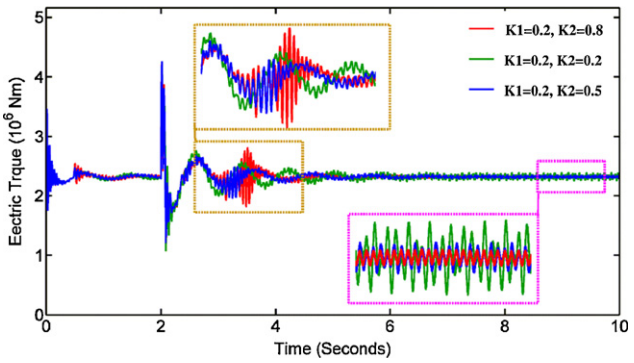

Fig. 20. Effect of gains variation on electric torque with CPC for the resistive fault (Case I).

inductive faults for both the open loop and the CPC methodology are compared. As seen in these figures, the SSR using the CPC is more quickly damped than using the open loop control. Moreover, the LFPO damping time by this methodology is reduced significantly, and for example, as seen in Fig. 19, for the inductive fault it decreases from 7 s in the open loop control to about 2.5 s in the constant power control.

On the other hand, for Case I, which was unstable in the open loop control, although this methodology could damp the SSR and stabilize the system for a wide range of gains, it was not possible to regulate the gains (K_1, K_2) in such a way that the system response is acceptable. For example, by increasing K_2 (or K_1) in constant K_1 (or K_2), the system's oscillations in the steady state decreases, while some sub-synchronous oscillation appears in the system after around 1 s of fault clearing. Fig. 20 shows the problem for $K_1 = 0.2$ [degree/MW] and different values of K_2 when the resistive fault is applied at $t = 2$ s. Also, in Fig. 21, the best response for the inductive fault with the gains (0.2, 1) [degree/MW] is shown. As seen in this figure, although the electric torque is stabilized in this case, the 15 Hz sub-synchronous resonance appears in the system after the fault clearing and lasts for about 2 s.

So far, it has been shown that the CPC methodology is able to effectively damp both the SSR and LFPO in the large rating of the GCSC (Case III). Comparing the results obtained by this methodology for this case with all of the results for all cases (I–III) in [11,12] for the same fault condition (the resistive fault) has shown the advantage of the developed control methodology. However, because this case leads to an increased power rating for the GCSC, it is not cost-effective. Moreover, although in Case I the SSR is totally damped for a wide range of the gains, it is not possible to regulate the gains in order to obtain a steady state performance with the minimum oscillation for the system while alleviating the subsynchronous resonance created at the first second of the fault's occurring. However, it would be better if the performance of Case I was close to the performance of Case III, resulting in a lower-cost

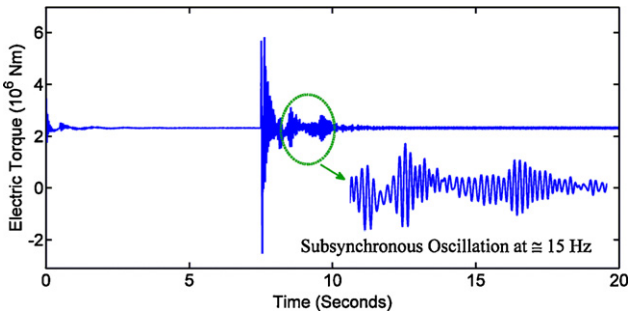

Fig. 21. Electric torque with CPC for the inductive fault (Case I).

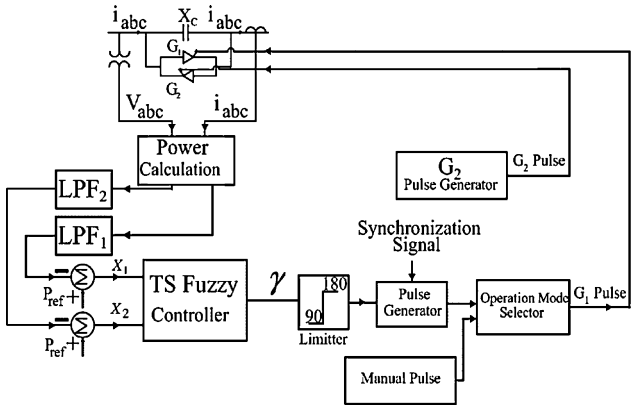

Fig. 22. GCSC with TS fuzzy control methodology.

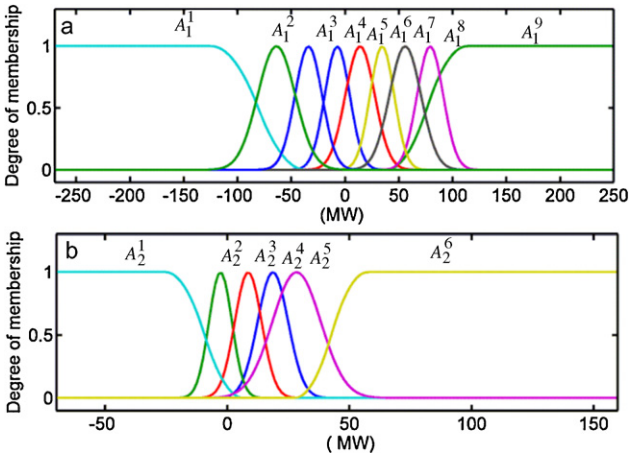

Fig. 23. Membership functions for (a) X_1 and (b) X_2.

configuration for the GCSC. In the following section, in order to reach this goal, a TS fuzzy control methodology is presented.

8. TS fuzzy control methodology

Recently, fuzzy logic controllers have generated a great deal of interest in various applications and have been introduced in the power electronics field [17–19] and SSR damping [20]. The advantages of fuzzy logic controllers over the conventional PI controller are that they do not need an accurate mathematical model; they can work with imprecise inputs, can handle nonlinearity, and may be more robust than the conventional PI controller [21]. In this section, a TS fuzzy control methodology is presented to solve the problem of the CPC in Case I.

Fig. 22 shows the schematic diagram of the GCSC turn-off angle control based on this methodology. In this figure, the TS fuzzy logic controller is replaced with the gains (K_1, K_2) in Fig. 16. The outputs of LPF$_1$ and LPF$_2$ (X_1 and X_2), after being compared with the power order, are used as inputs for fuzzy processing. The output of the TS fuzzy controller is the GCSC's turn-off angle (γ) which after being passed through a limiter is fed to a pulse generator block synchronized by the line's current zero crossing to produce the GCSC input pulse. The design process of the TS fuzzy logic controller (FLC) is described as follows.

8.1. Fuzzification

Fuzzification is the process of finding appropriate membership functions to describe crisp data. In this paper, the control rules and membership functions were obtained by trial-and-error method. So the results of the GCSC CPC methodology for different gains were studied. Then, based on these results, the appropriate membership functions and the control rules were determined. The membership functions for fuzzy controller inputs are shown in Fig. 23. The equation of the Gaussian membership used to determine the grade of membership values is as follows:

$$\mu_{A_i^j}(X_i, C_i^j, \sigma_i^j) = \exp\left(\frac{-(X_i - C_i^j)}{(2\sigma_i^j)^2}\right) \tag{4}$$

where A_i^j is the Gaussian membership function, $\mu_{A_i^j}$ is the value the membership grade, X_i is the TS fuzzy controller input, and C_i^j and σ_i^j are the mean value and variance of the Gaussian membership function, respectively.

8.2. Fuzzy rule base

The rule base is the heart of a fuzzy controller. The controller has two inputs, X_1 and X_2 which as seen in Fig. 23 were represented by nine and six membership functions, respectively. Therefore, the TS fuzzy controller uses 54 rules as follows:

$$\text{If } X_1 = A_1{}^j \text{ and } X_2 = A_2{}^j, \quad \text{then } Z_m = K_{1n}X_1 + K_{2n}X_2 + \gamma^*, \quad m = 1, 2, \ldots, 54 \tag{5}$$

where A_1^j and A_2^j are fuzzy sets related to the TS fuzzy logic controller inputs X_1 and X_2, respectively. Also, Z_m represents the consequent of the TS fuzzy controller in the mth "If-Then" rule, and γ^* is the reference turn-off angle that in this study was considered 113.5°, as mentioned in Section 5. Also, the proper values of (K_{1n},K_{2n}) were chosen by studying the results of the CPC methodology in different situations, before and after fault, in order to obtain the system steady state performance with the minimum oscillation and eliminate the sub-synchronous resonance occurring at around 1 s of fault clearing.

8.3. Fuzzy inference

The basic operation of the inference engine is that it infers, i.e. it deduces from evidence or data a logical conclusion. Here, Zadeh's rule for the "And" operation is used [22].

8.4. Defuzzification

In this part, the fuzzy conclusion of the inference engine is defuzzified, i.e. it is converted into a crisp signal. The mentioned signal is the final product of the FLC, which is the crisp control signal to the process. The output level Z_m of each rule is weighted by the firing strength W_m of the rule as follows:

$$W_m = Andmethod(\mu_{A_1}^j(X_1), \mu_{A_2}^j(X_2)), \quad m = 1, 2, \ldots, 54. \tag{6}$$

The final output of the system is the weighted average of all rule outputs, computed by (7).

$$\text{Final output} = \frac{\sum_{m=1}^{54} W_m Z_m}{\sum_1^{54} W_m}. \tag{7}$$

8.5. Simulation results and discussions

Similar to the other control methodologies, the simulation of the system shown in Fig. 10 with the TS fuzzy control method-

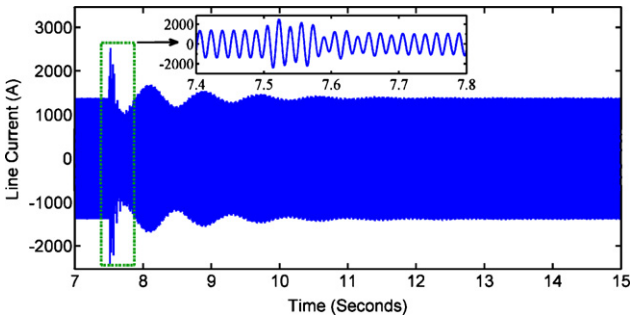

Fig. 24. Line current with TS fuzzy control for resistive fault (Case I).

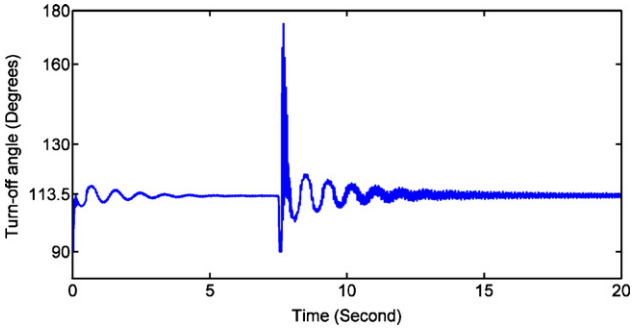

Fig. 25. Applied turn-off angle to the GCSC for the inductive fault (Case I).

ology was started with an ideal voltage source at the generator side, and then the ideal voltage source was substituted with a synchronous generator driven by the turbine. To examine the efficiency of this controller with different types of faults, both fault types were applied at bus B in Fig. 10 at $t = 7.5$ s. The resistive fault increased the line current from 1 to about 1.85 p.u., and the inductive fault increased the line current from 1 to about 3.8 p.u. In Fig. 24, the line current response for the resistive fault is shown. Also, in Fig. 25, the turn-off angle that is applied by the fuzzy controller to the GCSC for the inductive fault is depicted. This figure shows that after the fault the turn-off angle reaches its steady state condition (113.5°).

Fig. 26 compares the electric torque response for both Cases III and I for the resistive fault. As seen in this figure, using the fuzzy control methodology, the performance of the system in Case I has reached that of Case III with the CPC methodology. As a result, since in Case I the power rating of the GCSC is reduced, using the presented TS fuzzy control methodology for the GCSC will lead to a cost-effective solution for the SSR and LFPO damping. In fact, the controlling mechanism of CPC methodology is the main reason of damping both the SSR and LPFO at different GCSC ratings, and the

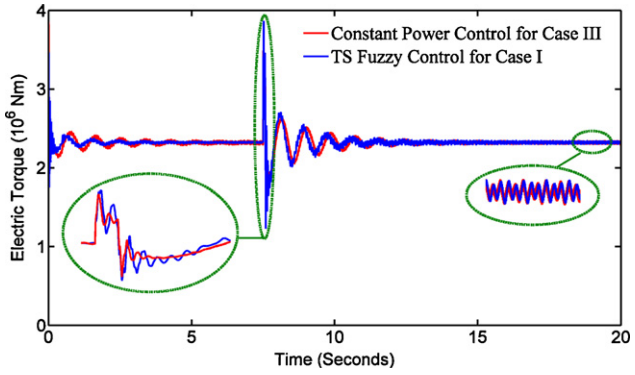

Fig. 26. Electric torque for the resistive fault: GCSC with CPC (Case III) and TS fuzzy control (Case I).

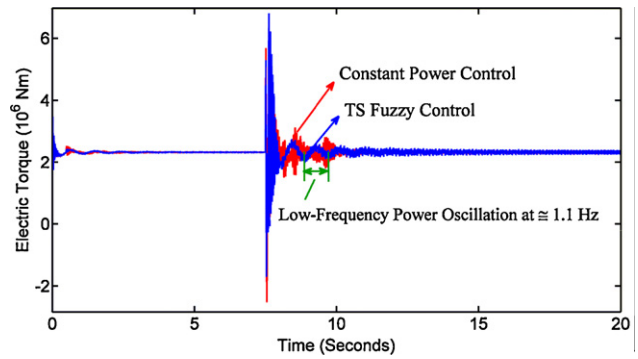

Fig. 27. Electric torque for inductive fault: GCSC with CPC (Case I) and TS fuzzy control (Case I).

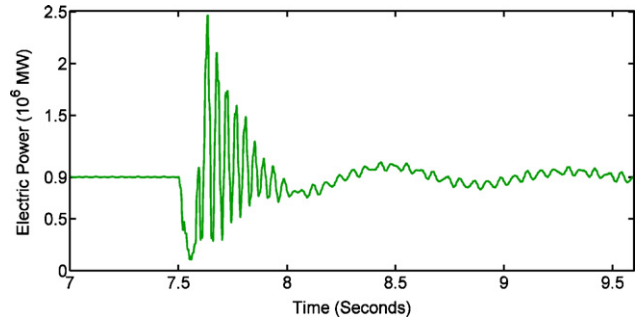

Fig. 28. Electric power detailing the initial transient with TS fuzzy control for inductive fault (Case I).

role of TS fuzzy control is to optimize the parameters of CPC to obtain more satisfactory results.

In Fig. 27, the electric torque response for the inductive fault for both the CPC and the TS fuzzy control for Case I is shown. Using the CPC, the SSR is totally damped; however, some SSR appears in the system after 1 s of fault clearing. Using the TS fuzzy control, as seen in Fig. 27, the SSR that appears in the electric torque response is eliminated. This figure also shows that using the TS fuzzy control methodology, a LFPO appears in the system at frequency around 1.25 Hz, as shown in Table 1, and it is damped in less than 2 s. In fact, the different tracking speed and dynamic precision of two different control systems that makes the disparity damping performance. This figure shows the effectiveness of the TS fuzzy control methodology in SSR and LFPO damping even with very intensive inductive fault.

These good responses can be explained using the simulation results shown in Figs. 28 and 29. In Fig. 28, the electric power response of the system is shown, and in Fig. 29 the corresponding turn-off angle is shown, detailing the initial transient corresponding to Fig. 27. As seen in these figures, when the electric power is

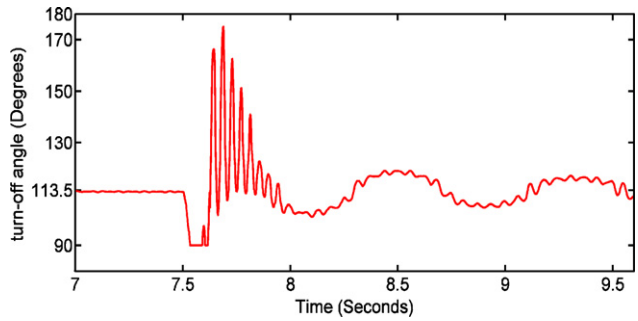

Fig. 29. GCSC turn-off angle corresponding to Fig. 27.

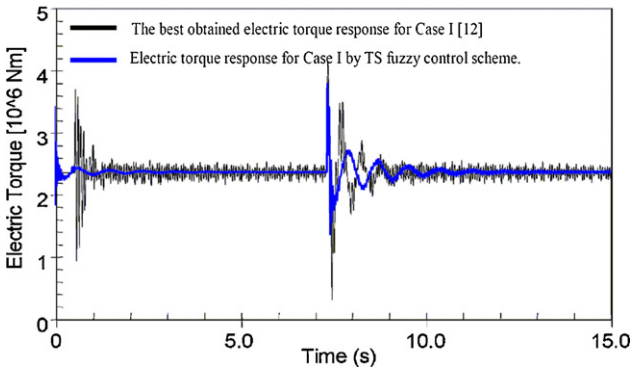

Fig. 30. Performance comparison with [12] for Case I.

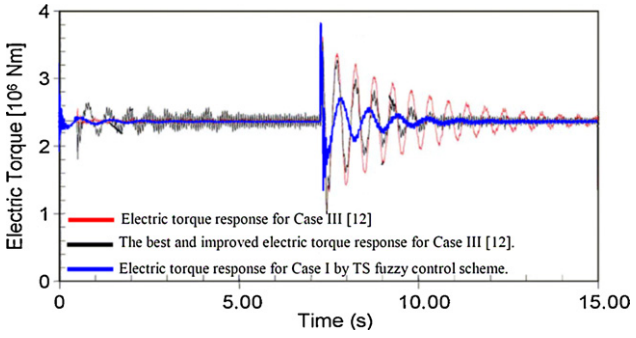

Fig. 31. Performance comparison for the Case III [12] and Case I.

increased, the turn-off angle is also increased, and consequently the compensation level is decreased and vice versa.

8.6. Performance comparison

In the previous subsection discussion, it was shown that the TS fuzzy control methodology provides an appropriate and cost-effective solution for the SSR and LFPO damping. To validate this result, in this section a comparative study between the response obtained by this methodology for Case I and the best response for Cases I and III obtained [9–11] is carried out. It is noted that in these references, the power system study model was the IEEE FBM, and the most intensive fault was similar to the resistive fault applied in this paper. Fig. 30 compares the electric torque response for the same case. As seen in this figure, the oscillation magnitude in the TS fuzzy control methodology is reduced, and the steady state response of the system also is improved. In Fig. 31, this comparison is carried out between Case I in this paper and Case III in [12]. This figure clearly shows that the response of the small GCSC (Case I) using the TS fuzzy control methodology is much better than that of the large GCSC (Case III) presented in [12]. These results confirm the effectiveness of the TS fuzzy control methodology.

9. Conclusion

This work has shown the impact of different GCSC control methodologies and ratings on the SSR and LFPO damping in a highly unstable power system. Three different control methodologies are proposed, and the impact of them on the SSR and LFPO damping are analyzed using two different GCSC ratings (the small and the large ratings). The dynamic performance results have shown that the GCSC device operating in the open loop control methodology can damp the SSR, but only in the large GCSC rating, resulting in a high-cost configuration for the GCSC. Also, the LFPO damping time in this methodology is too long. A CPC methodology is proposed to improve the operation of the GCSC in the open loop control methodology. It is shown that this methodology improves the performance of the large GCSC rating in both the SSR and LFPO damping. Furthermore, using this methodology, the small GCSC rating is also able to damp the SSR, but the dynamic performance of the system in this case is not desire. Finally, to enable the GCSC to damp both the SSR and LFPO using the small GCSC rating appropriately, a TS fuzzy control methodology is proposed. Simulation results have shown that the proposed TS fuzzy control methodology is able to guarantee the SSR and power oscillation damping even with the small GCSC rating. Therefore, since in the small GCSC rating the power rating of the GCSC is decreased, a TS fuzzy controlled GCSC will lead to a cost-effective solution for the SSR and LFPO damping. Performance comparison with other research groups confirms the effectiveness and the accuracy of the proposed TS fuzzy control methodology.

References

[1] IEEE SSR Working Group, Terms, definitions and symbols for subsynchronous oscillations, IEEE Trans. Power Appl. Syst. PAS-104 (June (6)) (1985) 1326–1334.
[2] IEEE SSR Task Force, First benchmark model for computer simulation of subsynchronous resonance, IEEE Trans. Power Appl. Syst. PAS-96 (September/October) (1997) 1562–1572.
[3] K. Padiyar, N. Prabhu, Design and performance evaluation of subsynchronous damping controller with STATCOM, IEEE Trans. Power Deliv. 21 (July (3)) (2006) 1398–1405.
[4] M. Bongiorno, L. Ängquist, J.S. Lennart, A novel control strategy for subsynchronous resonance mitigation using SSSC, IEEE Trans. Power Electron. 23 (April (2)) (2008) 1033–10041.
[5] M. Bongiorno, J. Svensson, L. Ängquist, On control of static synchronous series compensator for SSR mitigation, IEEE Trans. Power Electron. 23 (March (2)) (2008) 735–743.
[6] W. Bo, Z. Yan, Damping subsynchronous oscillation using UPFC—a FACTS device, in: Proc. Int. Conf. Power System Technology, vol. 4—PowerCon 2002, October 13–17, 2002, pp. 2298–2301.
[7] L.A.S. Pilotto, A. Bianco, W.F. Long, A.A. Edris, Impact of TCSC control methodologies on subsynchronous oscillations, IEEE Trans. Power Deliv. 18 (January (1)) (2003) 243–252.
[8] G.G. Karady, et al., Continuously regulated series capacitor, IEEE Trans. Power Deliv. 8 (July (3)) (1993) 1348–1354.
[9] L.F.W. Souza, E.H. Watanabe, J.E.R. Alves Jr., Thyristor and gate-controlled series capacitors: a comparison of components rating, IEEE Trans. Power Deliv. 23 (2, Apr) (2008) 899–906.
[10] F.D. Jesus, E.H. Watanabe, L.F.W. Souza, J.E.R. Alves Jr., Analysis of SSR mitigation using gate-controlled series capacitors, in: Proc. 36th IEEE Power Electronics Specialists Conf. (PESC 2005), Recife, Brazil, June, 2005, pp. 1402–1406.
[11] F.D. Jesus, E.H. Watanabe, L.F.W. Souza, J.E.R. Alves Jr., SSR mitigation using gare-controlled series capacitor, in: IEEE Power Engineering Society General Meeting (PES 2006), June, 2006.
[12] F.D. Jesus, E.H. Watanabe, L.F.W. Souza, J.E.R. Alves Jr., SSR and power oscillation damping using gate-controlled series capacitor (GCSC), IEEE Trans. Power Deliv. 22 (July (3)) (2007) 1806–1812.
[13] H.A. Mohammadpour, S.M.H. Mirhosseini, A. Shoulaie, Comparative study of proportional and TS fuzzy controlled GCSC for SSR mitigation, in: IEEE Second International Conference on Power Engineering, Energy and Electrical Drives, Lisbon, Portugal, March, 2009.
[14] H.A. Mohammadpour, M.R. Alizadeh Pahlavani, A. Shoulaie, On harmonic analysis of multi-module gate-controlled series capacitor (MGCSC) considering SSR phenomenon, Int. Rev. Electr. Eng. (IREE) 4 (August (4)) (2009) 627–634.
[15] H.A. Mohammadpour, M.R. Alizadeh Pahlavani, A. Shiri, A. Naghashpour, Voltage sag mitigation by means of gate-controlled series capacitor (GCSC), in: Proc. 1st IEEE International Conference on Electric Power and Energy Conversion Systems, American University of Sharjah, UAE, November, 2009.
[16] H.A. Mohammadpour, A. Shiri, R. Ghandehari, A. Naghashpour, Power quality issues in multi-module gate controlled series capacitor, in: Proc. 1st IEEE International Conference on Electric Power and Energy Conversion Systems, American University of Sharjah, UAE, November, 2009.
[17] B.K. Bose, Expert systems, in: Fuzzy Logic and Neural Network Applications in Power Electronics and Motion Control, IEEE Press, Piscataway, NJ, 1999 (Chapter 11).
[18] A. Dell'Aquila, A. Lecci, V.G. Monopoli, Fuzzy controlled active filter driven by an innovative current reference for cost reduction, Proc. IEEE Int. Symp. Ind. Electron. 3 (May) (2002) 948–952.
[19] K. Viswanathan, D. Srinivasan, R. Oruganti, Design and analysis of SISO fuzzy logic controller for power electronic converters, Proc. IEEE Int. Conf. Fuzzy Syst. (July (3)) (2004) 1293–1298.

[20] A. Shoulaie, M. Bayatipoodeh, Gh. Shahgholian, A.H. Zarei, Fuzzy logic controller for damping sub-synchronous oscillation in power system, in: International Conference on Intelligent and Advanced Systems, November, 2007, pp. 887–892.
[21] C.N. Bhende, S. Mishra, S.K. Jain, TS fuzzy-controlled active power filter for load compensation, IEEE Trans. Power Deliv. 21 (June (3)) (2006) 1459–1465.
[22] W.L. Xin, A Course in Fuzzy Systems and Control, Prentice Hall, 1996 (Paperback, published August).

Mohammad Reza Alizadeh Pahlavani was born in Iran in 1974. He received his Ph.D. degree in electrical engineering at the Iran University of Science and Technology (IUST) in 1998, 2002, and 2009, respectively. He is the author of more than fifty journal and conference papers in the field of electromagnetic systems, electrical machines, power electronics, FACTS devices, and pulsed power.

Hossein Ali Mohammadpour was born in Iran in 1982. He received the B.Sc. and M.Sc. degrees from the Iran University of Science and Technology (IUST), Tehran, Iran, in 2006 and 2009, respectively. He is currently a Ph.D. student in the Department of Electrical Engineering, University of South Carolina, Columbia. His current areas of research interests include power systems dynamics and control, power electronics and applications, FACTS devices, and electromagnetic systems.